Assessing the quasi-static conditions for shearing in granular media within the critical state soil mechanics framework

Assessing the quasi-static conditions for shearing in granular media within the critical state soil mechanics framework

J. C. Lopera Perez[1], C. Y. Kwok[1], C. O'Sullivan[2], X. Huang[1,2,3] & K. J. Hanley[3,4]

[1]*Department of Civil Engineering, The University of Hong Kong, Haking Wong Building, Pokfulam Road, Hong Kong*

[2]*Department of Civil and Environmental Engineering, Imperial College London, Skempton Building, London SW7 2AZ, UK*

[3]*Department of Geotechnical Engineering, Tongji University, Shanghai 200092, China*

[4]*Institute for Infrastructure and Environment, School of Engineering, The University of Edinburgh, Edinburgh EH9 3JL, United Kingdom*

Abstract

There has been a marked increase in the use of the discrete element method (DEM) in geomechanics in recent years. The way in which DEM simulations are set up can have a noticeable influence on the observed response. Here the conditions for quasi-static shearing in DEM simulations of granular materials were studied within the critical-state framework of soil behaviour. Thirty two constant-p' triaxial simulations were carried out from which critical-state relationships were defined in the void ratio-mean effective stress and deviator fabric-mechanical coordination number planes. Clear trends were observed in the void ratio, coordination number and deviatoric fabric at the critical state as the inertial number, *I*, was varied. The critical state relationships are aligned along distinct loci for each value of *I*. The critical state framework is used to show that there is an upper bound to the *I* values below which the simulation is quasi-static and the observed behaviour is independent of strain rate. The parameter *I* is shown to be a useful measure to assess the quality of quasi-static DEM simulations.

Keywords: Discrete element modelling; fabric/structure of soils; particle-scale behaviour; triaxial tests (IGC : D3/D6/E13).

1. Introduction

Significant, fundamental insight into the mechanics underlying the observed complex, non-linear response of granular materials can be gained via numerical simulations using the Discrete Element Method (DEM) (Cundall & Strack, 1979). Under quasi-static conditions there is no strain rate dependency; establishing general guidelines for the strain rate and material properties required to achieve this is important. Cundall & Strack (1979) suggested that in order to achieve quasi-static conditions, a strain rate should be chosen so that the inertial forces are smaller than the contact forces. In practice, however, a parametric study is often carried out to select the strain rate below which a consistent response is obtained. Many published research studies do not clearly state the value of the strain rate adopted. Hanley *et al* (2013) showed that there is a clear sensitivity of the stress-strain response of constant-volume DEM simulations to strain rate; thus, it is evident that attention should be paid to this matter.

The transition from the quasi-static regime where the inertial effect is negligible to the dynamic regime where the inertial effect is significant has been studied widely both numerically (MiDi, 2004; da Cruz *et al* 2005; Hatano, 2007; Agnolin & Roux, 2007; Peyneau & Roux, 2008; Koval *et al*, 2009; Radjai & Dubois, 2011; Gimbert *et al*, 2013; Azema *et al*, 2014) and experimentally (Kuwano *et al*, 2013). Many of these studies used a dimensionless parameter called the inertial number $I = \dot{\varepsilon} d\sqrt{\rho/p'}$, to identify different flow regimes, where $\dot{\varepsilon}$ is the shear rate, d is the mean size of grains in the assembly, ρ is the grain density, and p' is the mean effective stress (da Cruz *et al*, 2005). I quantifies inertia effects by considering the ratio of the inertial forces to the imposed forces: small values of I correspond to a quasi-static regime, intermediate values of I indicate dense flow, while large values of I indicate a collisional dynamic regime (da Cruz *et al* 2005). Prior studies have focussed on determining the characteristic values of I that separate these quasi-static, dense flow, and dynamic regimes, often using plane shear tests. For example, the boundary between the quasi-static and dense flow regimes varies between I < 1e-4 and I < 1e-1 (Macaro & Utili, 2012; Kuwano *et al*, 2013). This study aims to extend these findings from a soil mechanics perspective by investigating the effect of I on the critical state locus (CSL) at both macro and particle-scales, and to propose an upper limit of I that defines the quasi-static state regime when simulating soil mechanics element tests.

DEM simulations of triaxial tests under a range of initial densities and confining pressures were performed; in each simulation, I was maintained constant throughout the shearing stage. Critical state lines in the e-$(p'/p_a)^{\alpha}$ plane were identified for each I value considered. The critical state relationships were also explored at the particle scale by considering the coordination number and the deviatoric fabric.

2. DEM simulations

Three-dimensional simulations were carried out using a modified version of the open-source code LAMMPS (Plimpton, 1995). The particle size distribution (PSD) of the numerical assemblies (given in Figure 1) approximates that of Toyoura sand (Huang *et al*, 2014a). An initially non-contacting cloud of 10,624 particles enclosed by periodic boundaries was generated and then isotropically compressed to various combinations of void ratio and stress state as summarized in Table 1. The initial density was controlled by changing the inter-particle friction coefficient (μ) during the isotropic compression stage. After the target isotropic stress had been reached, the specimen was then subjected to numerical cycling until *p'* and the number of contacts became constant, indicating equilibrium. μ was subsequently changed to 0.25 which is the value used during shearing. Additional cycles were performed to ensure equilibrium before shearing commenced. Four samples were created at confining pressures ranging from 100 kPa to 5,000 kPa with the void ratio ranging from loose to medium dense.

Following isotropic compression, the samples were sheared under constant *p'* conditions which gave a constant value of *I* throughout the shearing process, where *I* was calculated using the strain rate applied in the direction of the major principal stress ($\dot{\varepsilon}_1$). $\dot{\varepsilon}_1$ was specified to give eight different values of *I* ranging from 5e-4 to 5e-1 as shown in Table 1. A servo-control algorithm was implemented that determined the $\dot{\varepsilon}_3$ needed to keep the constant-*p*' conditions and thus $\dot{\varepsilon}_3$ varied during the shearing stage. The minimum and maximum strain rates in the direction of σ'_3 ($\dot{\varepsilon}_3$) are also included in Table 1. If $\dot{\varepsilon}_3$ were to be considered in the definition of *I* (i.e. the absolute value of $\dot{\varepsilon}_3$), *I* could not be kept constant throughout the shearing stage. In previous contributions (i.e. MiDi, 2004; da Cruz *et al*, 2005) the definition for shear rate corresponds to the strain rate in the loading direction ($\dot{\varepsilon}_1$) as adopted in the present study. The loading condition applied to the system is shown in Figure 2. A simplified Hertz-Mindlin contact model was used with a shear modulus (*G*) of 29 GPa, particle Poisson's ratio (v) of 0.12 and particle density (ρ) of 2650 kg/m^3. A local damping coefficient of 0.1 was used in all simulations and gravity was not considered in these periodic cell simulations.

The input values adopted for the shear modulus and Poisson's ratio are consistent with the range of elastic properties of quartz (Simmons & Brace, 1965). Similar values of Poisson's ratio have been used by other studies (Ng, 2009; Huang *et al*, 2014a). For real quartz particles, the friction values are in the range of 0.12 – 0.35 as was observed by Senetakis *et al* (2013). Furthermore, it was reported by Huang *et al* (2014b) that using an interparticle friction coefficient higher than 0.5 together with a simplified Hertz-Mindlin contact model will result in a non-physical response.

One of the key assumptions of DEM simulations is that particles are treated as rigid bodies, which are allowed to overlap with other particles at the contact points. Therefore, all overlaps should be small in

relation to the particle sizes and thus a maximum overlap ratio of 5% can be considered as an appropriate limit as suggested by Itasca Consulting Group (2007).

3. Overall response

Figures 3(a) and (b) show the variation of stress ratio $\eta = q/p'$ (q is the deviatoric stress) and volumetric strain (ε_v) respectively with the major principal strain (ε_1) for a representative set of simulations with p' = 100 kPa and initial void ratio (e_0) of 0.616. All of these simulations indicate a material response typically representative of dense or medium dense samples. At a given strain level, both ε_v and η vary systematically with I. After an initial contraction during the first 5% of axial strain, samples sheared at higher strain rates (large I) tend to dilate more. For the case of I = 5e-1, there is no initial contraction and the samples dilate throughout shearing. Samples sheared with $I \leq$ 2.5e-3 give indistinguishable volumetric responses reaching the same value of ε_v at the critical state. Referring to Figure 3(a), the peak and critical state values of η both decrease as I decreases. Although some fluctuations are present, samples sheared with $I \leq$ 2.5e-3 show a very similar response in η both at the initial peak and at the critical state. A similar dependence of ε_v upon I was found for all other p' values; however, the response characteristics at higher stress levels were close to those of loose samples.

Figure 4 presents the variation of η with dilatancy ($D = d\varepsilon_v/d\varepsilon_q$) for the case of p' = 100 kPa, e_0 = 0.616 in Figure 4(a) and for the case of p' = 5000 kPa, e_0 = 0.596 in Figure 4(b). D was calculated from the total strains using a central-difference approach (Been & Jefferies, 2004), considering the elastic strain components to be negligible. Figure 4 shows a consistent response with higher η attained at negative values of dilatancy regardless of I. For the two levels of p' considered, the stress-dilatancy relationships are indistinguishable for simulations with $I \leq$ 2.5e-3.

4. Critical state response

a. Macro-mechanical response

Figure 5(a) illustrates the variation of the critical state η value with I; each η value was obtained from a set of five simulations, each set with different p' values. It is clear that when $I >$ 1e-2, η increases as I increases; however, η is not sensitive to I for values of $I \leq$ 1e-2. These data agree with prior 2D (da Cruz *et al,* 2005) and 3D planar shear simulations (Azema *et al,* 2014). Figure 5(b) shows the variation of e_{cs} (the void ratio at the critical state) with I for the p' values considered. For a given p', the value of e_{cs} remains almost constant when $I \leq$ 2.5e-3. When $I >$ 2.5e-3, e_{cs} increases with I. Figure 5(c) gives the e_{cs}-$(p'/p_a)^{0.7}$ relationship and the data for each I value is seen to follow the linear relationship suggested by Li & Wang (1998), i.e., $e_{cs} = \Gamma - \lambda(p'/p_a)^{\alpha}$, where Γ is the intercept of CSL, λ is the slope of the CSL, p_a is atmospheric pressure (101.325 kPa) and the α value of 0.7 suggested

for Toyoura sand by Li & Wang (1998) is used. Note that each data point was taken as the values of e and p' averaged over the last 10% to 20% of axial strain due to fluctuations in the load-deformation response. The CSLs move downwards with decreasing I when $I \geq$ 2.5e-3 and the CSLs do not vary noticeably when $I \leq$ 2.5e-3. The CSL parameters Γ and λ are presented in Figure 5(d) for the different sets of simulations. Both Γ and λ decrease with I and constant values of Γ and insignificant variations of λ can be observed for samples sheared at $I \leq$ 2.5e-3.

b. Micro-mechanical response

In an attempt to understand the physical basis for the variation in sensitivity of the overall load-deformation response to I, two particle-scale parameters were analysed: the structural anisotropy (fabric) using the fabric tensor defined by Satake (1982) as:

$$\Phi_{ij} = \frac{1}{N_c}\sum_{1}^{N_c} n_i n_j \quad (1)$$

where N_c is the total number of contacts and n_i is the unit contact normal. The largest, intermediate and smallest eigenvalues of the fabric tensor are denoted as Φ_1, Φ_2 and Φ_3 respectively. The deviatoric fabric, Φ_1- Φ_3, describes the degree of structural anisotropy. A second parameter is the mechanical coordination number (Z_m) defined as the average number of contacts per particle excluding "rattlers" with zero or one contact (Thornton, 2000). As reported by Thornton (2000), samples at the same stress level with differing initial densities tend towards a unique Z_m at large strain levels. For this data set (Φ_1- Φ_3) tends towards a unique critical value at large strain levels which is in line with the observations of Guo and Zhao (2013). Figure 6(a) shows (Φ_1- Φ_3) against Z_m at the critical state for different values of I. A linear relationship between (Φ_1- Φ_3) and Z_m is observed in all cases of I. It is also evident in Figure 6(a) that the loci move downwards with decreasing I, converging towards same values at $I \leq$ 2.5e-3. These data indicate that when the structural anisotropy is higher, fewer load bearing contacts exist in the system. The product of (Φ_1- Φ_3) and Z_m gives an indication of the intensity of the contacts acting in the orientation of the major fabric relative to that of contacts oriented in the minor fabric direction (Maeda et al, 2010). Figure 6(b) shows that this deviator fabric intensity depends on I. The data show that the deviator fabric intensity increases with I when $I \geq$ 1e-2. A more constant response of the deviator fabric intensity (Z_m*(Φ_1- Φ_3)) regardless of p' is observed when $I \leq$ 2.5e-3 showing a critical state structure independent of strain rate.

The connectivity, C, which reflects the number of contacts possessed by each particle (e.g., Shire and O'Sullivan, 2013) was also considered for all tests. The minimum value of C for a particle to be considered (statically) mechanically stable in a frictional system is four (Zhang & Makse, 2004). For this study, particles with $C \leq 3$ are considered unstable. Figure 7(a) illustrates the frequency of C for various I with p' = 100 kPa, e_0 = 0.616. Figure 7(b) shows the probability of occurrence of unstable

and stable particles against I for various values of p'. For I > 2.5e-3 the proportion of unstable particles increases with increasing I. The distribution of C values is not very sensitive to I for $I \leq$ 2.5e-3. Thus it seems that as I increases beyond 2.5e-3 the mechanical redundancy of the system is diminished; more particles are accelerating (i.e., the unbalanced forces / inertial effects are no longer negligible) and are thus not in a state of static equilibrium.

5. Conclusions

This research adds to previous studies by considering the sensitivity of the material response to the inertial number (I) within the critical state soil mechanics framework. Thirty two triaxial test simulations were performed in order to define an upper limit of I for quasi-static simulations independent of strain rate. I has been systematically controlled by specifying different values for the mean effective stress (p') and strain rate ($\dot{\varepsilon}$), allowing the effect of I be established. The data presented here can be used by DEM analysts to inform decisions about the appropriate strain rate for running DEM simulations of soil mechanics element tests.

A clear dependency of dilatancy on I was found for I > 1e-2 while an indistinguishable response was observed for the cases of $I \leq$ 2.5e-3. Considering the macro-mechanical critical state relationships, only those tests performed at values of $I \leq$ 2.5e-3 showed a response which is independent of strain rate (same CSL in the e_{cs}-$(p'/p_a)^{\alpha}$ plane); for higher I values the CSL position depends on I. In terms of the micro-mechanical parameters (Φ_1- Φ_3) and Z_m, the samples again exhibited a response independent of strain rate for values of $I \leq$ 2.5e-3. The data plotted in the (Φ_1- Φ_3) - Z_m plane showed a linear relationship. A critical state structure as noticed from the deviator fabric intensity was also found to be independent of strain rate from values of $I \leq$ 2.5e-3. Similarly there was a marked decrease in the number of particles that are statically redundant, i.e., that have four or more contacts when I > 2.5e-3.

From the results described above it is reasonable to propose a conservative upper limit for quasi-static simulations of I = 2.5e-3 that includes a strain-rate independent response from both macro and micro-mechanical perspectives. This contribution has demonstrated clearly the sensitivity of the observed stress:deformation response to the applied strain rate in DEM simulations while highlighting the usefulness of considering I as an indicator of quasi-static conditions when selecting a suitable strain rate. Choosing a strain rate based on I is more theoretically justifiable than a trial-and-error procedure varying the strain rate until a consistent response is achieved.

The upper limit proposed for quasi-static simulations is consistent with some of the available literature (MiDi, 2004; da Cruz *et al* 2005; Koval *et al*, 2009; Azema *et al*, 2014). This newly-

acquired data, combined with the existing data in the literature, seems to indicate that the critical I proposed to maintain quasi-static conditions is independent of initial density, type of test and number of particles. For drained and constant volume tests in which p', and consequently I, varies, attention should be paid so that the value of I does not exceed the limit proposed. Guo & Zhao (2014a) and Guo & Zhao (2014b) chose a strain rate for DEM simulations by considering a value of I below the limit proposed in this study. As a guidance for conducting conventional triaxial test using DEM, it is suggested that the strain rate applied in the direction of loading should be carefully chosen based on the $I \leq$ 2.5e-3 criterion using the expected minimum p' (i.e. p'_0 in a conventional drained simulation or p' at the phase transformation for undrained simulations).

Acknowledgements

The work presented in this study was conducted using the HKU information Technology Services research computing facilities that are supported in part by the Hong Kong UGC Special Equipment Grant (SEG HKU09).

References

Agnolin I. and Roux N. J. (2007) Internal states of model isotropic granular packings. I. Assembling process, geometry, and contact networks. *Phys. Rev.* E, 76, 061302

Azema E. and Radjai F. (2014) Internal structure of inertial granular flows. *Physical Review Letters* , 12, 078001

Been K. and Jefferies M. (2004) Stress-dilatancy in very loose sand. *Can. Geotech. J.* 41, 972 - 989

da Cruz F., Emam S., Prochnow M., J. N. Roux and F. Chevoir (2005) Rheophysics of dense granular materials: Discrete simulation of plane shear flows. *Phys. Rev.* E, 72, 021309

Cundall P. A. and Strack O. D. L. (1979) A discrete element model for granular assemblies. *Geotechnique* 29, No. 1, 47 – 65

Gimbert F., Amitrano D. and Weiss J. (2013) Crossover from quasi-static to dense flow regime in compressed frictional granular media. *EPL* 104, 46001

Guo N. and Zhao J. (2013) The signature of shear-induced anisotropy in granular media. *Comput. Geotech.* 47, 1 – 15

Guo N. and Zhao J. (2014a) Local fluctuations and spatial correlations in granular flows under constant-volume quasi-static shear. *Phys. Rev. E*, 89, 042208.

Guo N. and Zhao J. (2014b) A coupled FEM/DEM approach for hierarchical multiscale modelling of granular media. *Int. J. Numer. Meth. Engng*, 99, 789-818.

Hanley K. J., Huang X., O'Sullivan C. and Kwok C.Y. (2013) Challenges of simulating undrained tests using the constant volume method in DEM. *AIP Conference Proceedings* 1542, 277

Hatano T. (2007) Power-law friction in closely packed granular materials. *Phys. Rev.* E, 75, 060301

Huang, X., O'Sullivan, C., Hanley, K. J., Kwok, C.Y. (2014a) "DEM Analysis of the State Parameter", *Géotechnique* 64(12) 954 – 965

Huang, X., Hanley, K. J., O'Sullivan, C. & Kwok, C.Y. (2014b). Exploring the Influence of interparticle friction on critical state behaviour using DEM. Int. J. Numer. Anal. Met. 38 No. 12, 1276-1297.

Itasca Consulting Group (2007) PFC3D Version 4.0 User Manual. Minneapolis, MN, USA., Itasca Consulting Group.

Koval G., Roux J. N., Corfdir A. and Chevoir F. (2009) Annular shear of cohesionless granular materials: From the inertial to quasistatic regime. *Phys. Rev.* E, 79, 021306

Kuwano O., Ando R. and Hatano T (2013) Granular friction in a wide range of shear rates. *AIP Conference Proceedings* 1542, 32

Li X.S. and Wang Y. (1998) Linear representation of steady-state line for Sand. *J. Geomech. Geoenvironmental Eng*. 124, 1215–1217

Macaro G. and Utili S. (2012) DEM triaxial tests of a seabed sand. *Discrete Element Modelling of Particulate Media, The Royal Society of Chemistry*: 203 - 211

Maeda K., Sakai H., Kondo A., Yamaguchi T., Fukuma M. and Nukudami E. (2010) Stress-chain based micromechanics of sand with grain shape effect. *Granul. Matter* 12:499 – 505.

MiDi G. D. R. (2004) On dense granular flows. *Eur. Phys. J.* E 14, 341 – 365

Ng, T. (2009) Discrete element method simulations of the critical state of a granular material. *International Journal of Geomechanics*. 9 (5), 209-216.

Peyneau P. E and Roux J. N. (2008) Frictionless beads packs have macroscopic friction, but no dilatancy. *Phys. Rev.* E, 78, 011307

Plimpton S. (1995) Fast parallel algorithms for short-range molecular dynamics, *J. Comp. Phys.* 117, 1 – 19.

Radjai, F. and Dubois, F. (2011) *Discrete-element modelling of granular materials*. London, ISTE.

Satake M. (1982). Fabric tensor in granular materials. *In: Vermeer, P.A. and Luger, H.J. (eds.) IUTAM Symposium on Deformations and Failure of Granular Materials.* pp. 63–68. , Rotterdam: Balkema

Senetakis K., Coop, M.R. and Todisco, M.C. (2013) Tangential load-deflection behaviour at the contacts of soil particles. *Géotechnique Letters*, 3, No.2, 59-66

Shire T. and O'Sullivan C. (2013) Micromechanical assessment of an internal stability criterion. *Acta Geotech.* (2013) 8, 81-90

Simmons, G. & Brace, W.F. (1965) Comparison of Static and Dynamic Measurements of Compressibility of Rocks. Journal of Geophysical Research. 70 (22), 5649–5656.

Thornton C. (2000) Numerical simulations of deviatoric shear deformation of granular media. *Géotechnique*. **50**, No. 1, 43–53.

Zhang H.P. and Makse H.A. (2005) Jamming transition in emulsions and granular materials. *Phys Rev* E, 72, 011301

Notation

d	Particle diameter
D	Dilatancy $D = d\varepsilon_v/d\varepsilon_q$
e	Void ratio
e_0	Initial void ratio
e_{cs}	Void ratio at the critical state
G	Particle shear modulus
I	Inertial number
p'	Mean effective stress
p_0'	Mean effective stress after isotropic compression
q	Deviatoric stress
Z_m	Mechanical coordination number
Γ	Intercept of the critical state line in the e-$(p'/p_a)^{0.7}$ space with axis $p' = 0$
$\dot{\varepsilon}$	Strain rate
ε_1; ε_2; ε_3	Major, intermediate and minor principal strains ($\varepsilon_2 = \varepsilon_3$)
ε_v	Volumetric strain
η	Stress ratio $\eta = (q/p')$
ε_q	Shear strain $\varepsilon_q = 2/3(\varepsilon_1 - \varepsilon_3)$
λ	Slope of the critical state line in the e_{cs}-$(p'/p_a)^{0.7}$ space
μ	Inter-particle friction coefficient
v	Particle Poisson's ratio
ρ	Particle density
σ'_1; σ'_2; σ'_3	Major, intermediate and minor principal stresses ($\sigma'_2 = \sigma'_3$)
$(\Phi_1 - \Phi_3)$	Deviatoric fabric

Figure

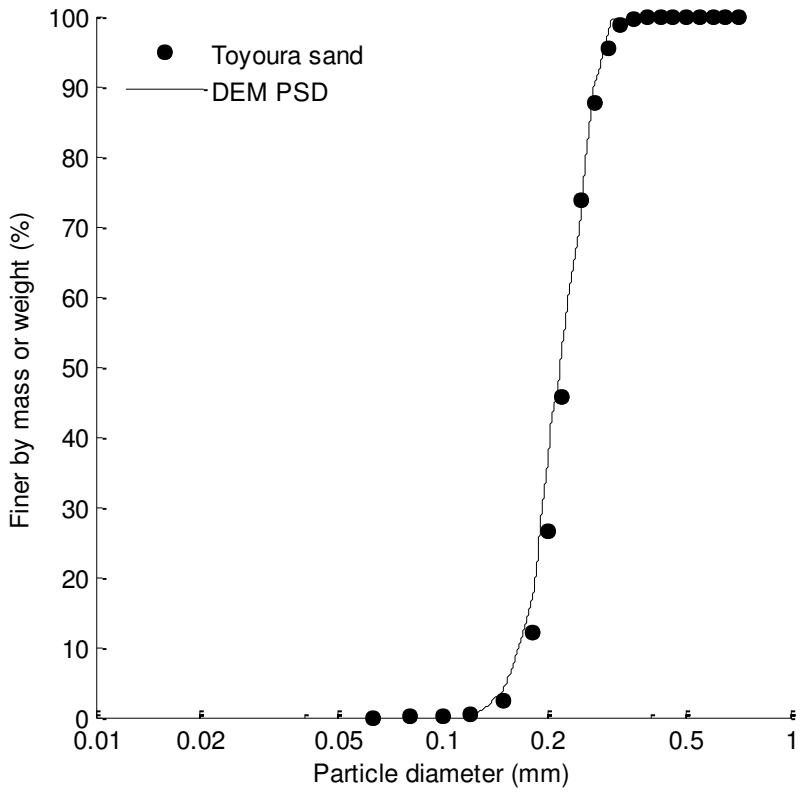

Figure 1. Particle size distribution of numerical samples compared with laboratory data for Toyoura sand

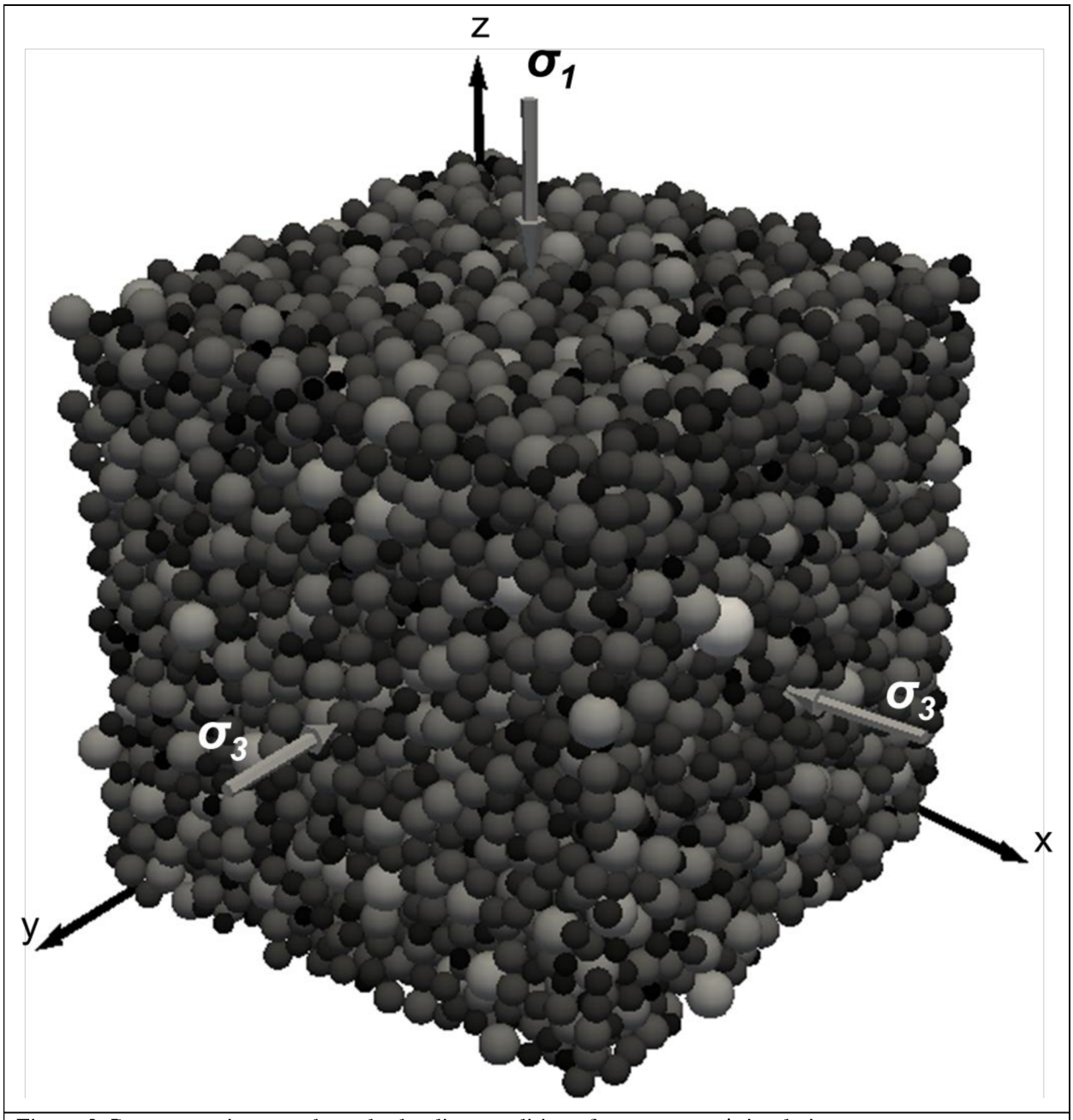

Figure 2. Representative sample under loading conditions for constant *p'* simulations.

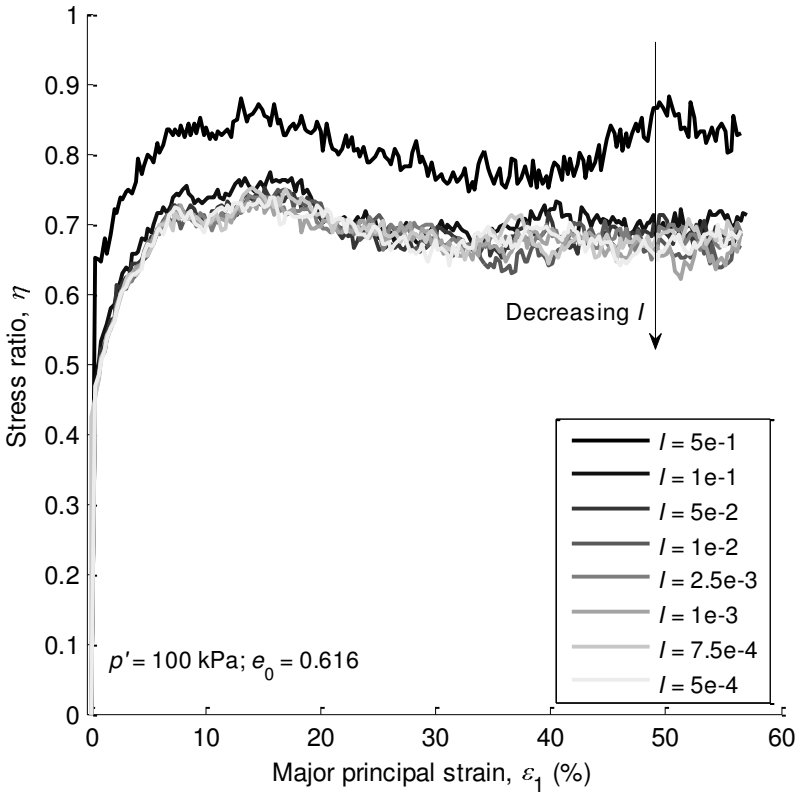

(a) Stress ratio against major principal strain (p' = 100 kPa, e_0 = 0.616)

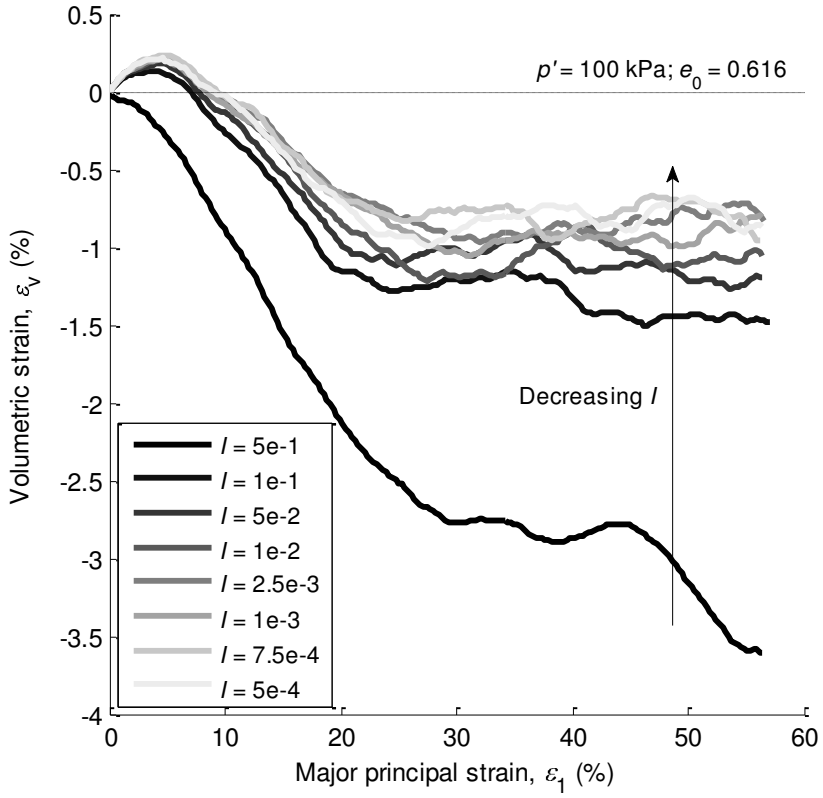

(b) Volumetric strain against major principal strain (p' = 100 kPa, e_0 = 0.616)

Figure 3. Overall response of the numerical sample for various values of I.

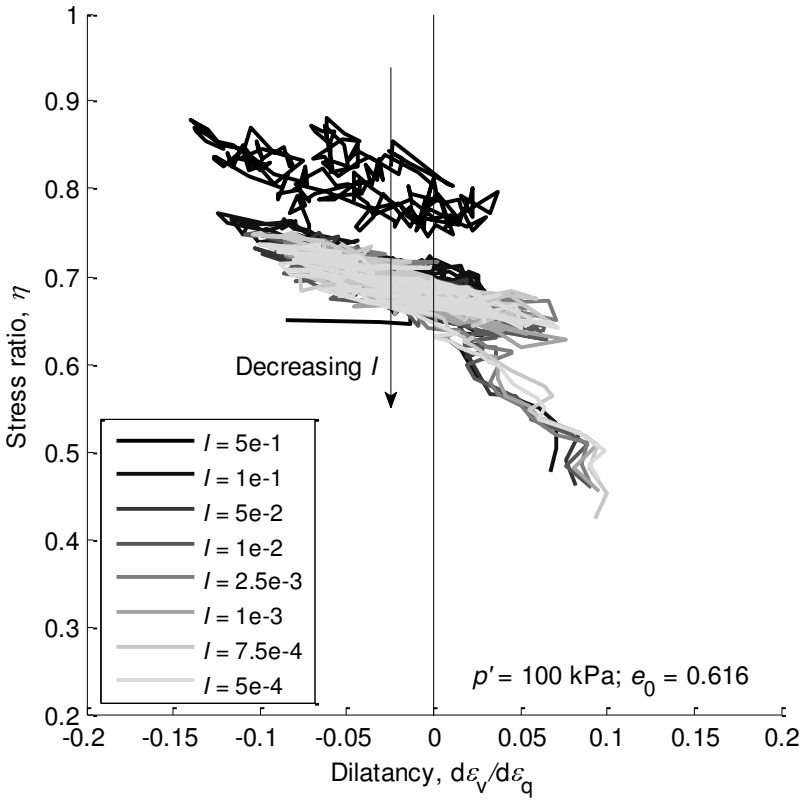

(a) Stress-dilatancy relationship (p' = 100 kPa, e_0 = 0.616)

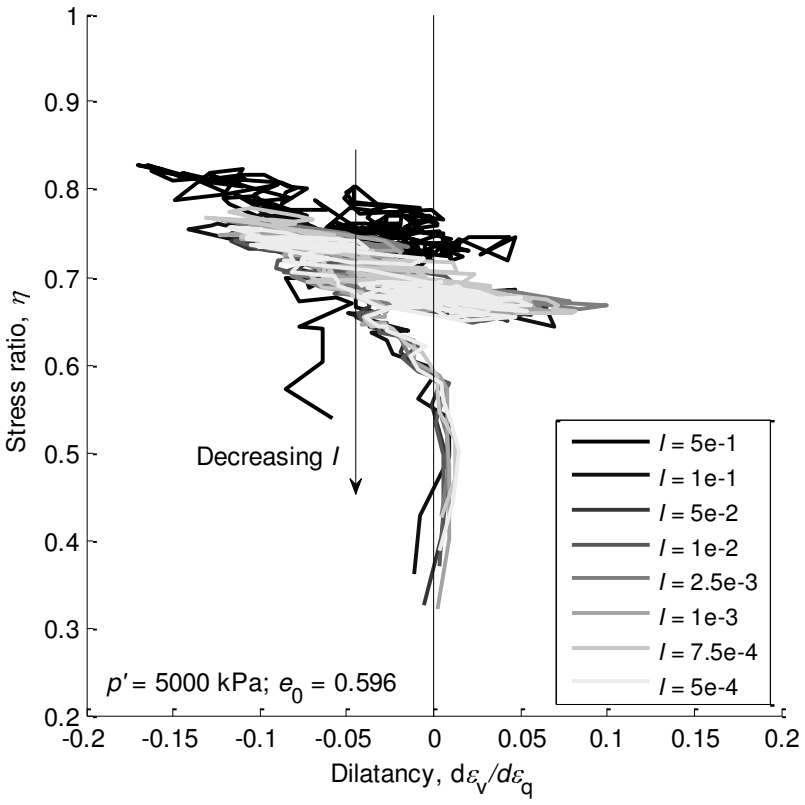

(b) Stress-dilatancy relationship (p' = 5000 kPa, e_0 = 0.596)

Figure 4. Stress-dilatancy relationships

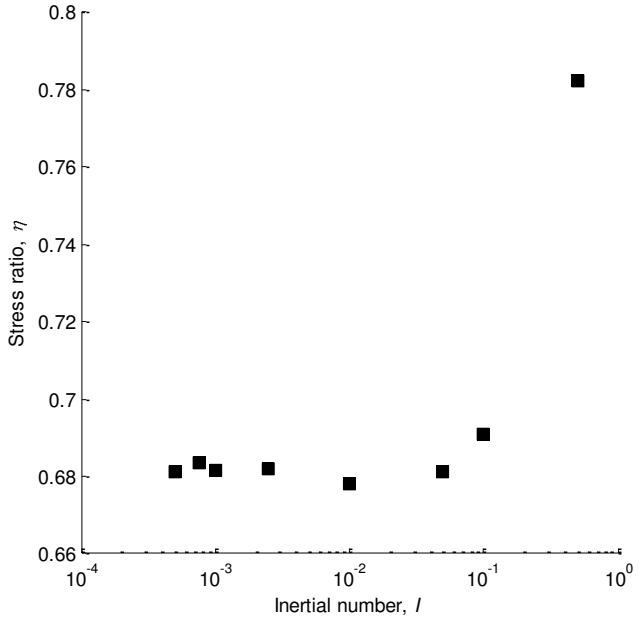

(a) Stress ratio at critical state for different levels of I

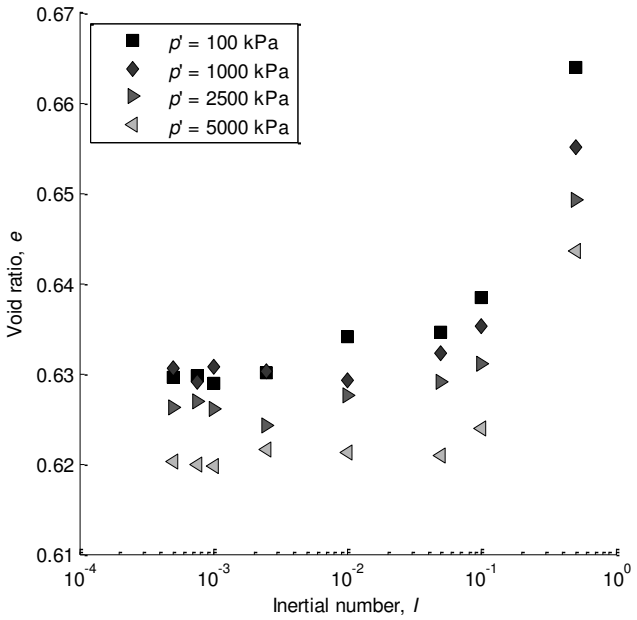

(b) Void ratio at critical state for different values of I and p'.

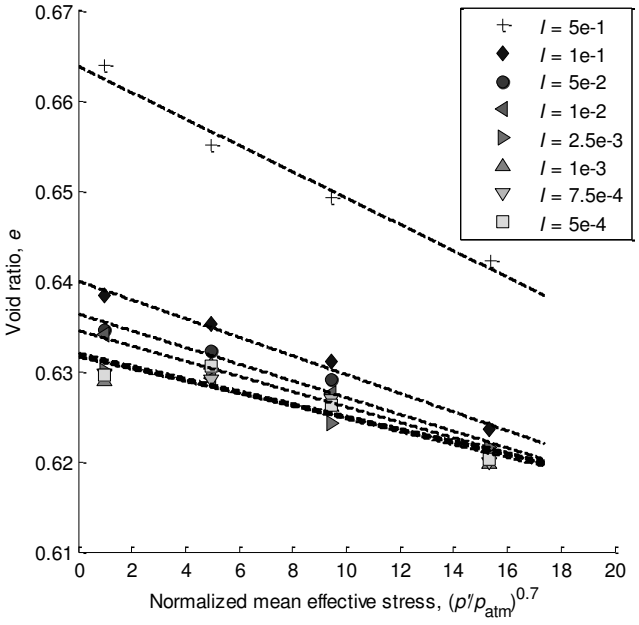

(c) CSL in the e-$(p'/p_a)^{0.7}$ space

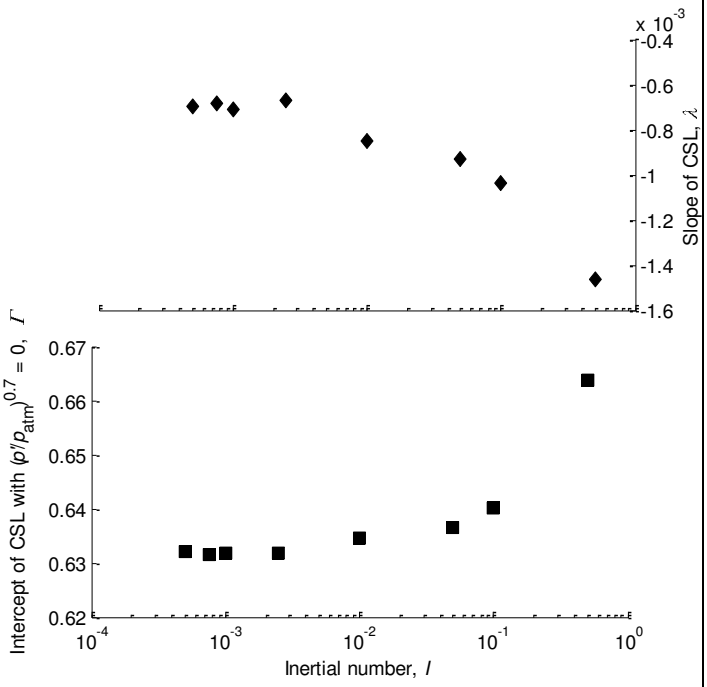

(d) CSL line parameters for different I

Figure 5. Macro-scale analysis of the critical state

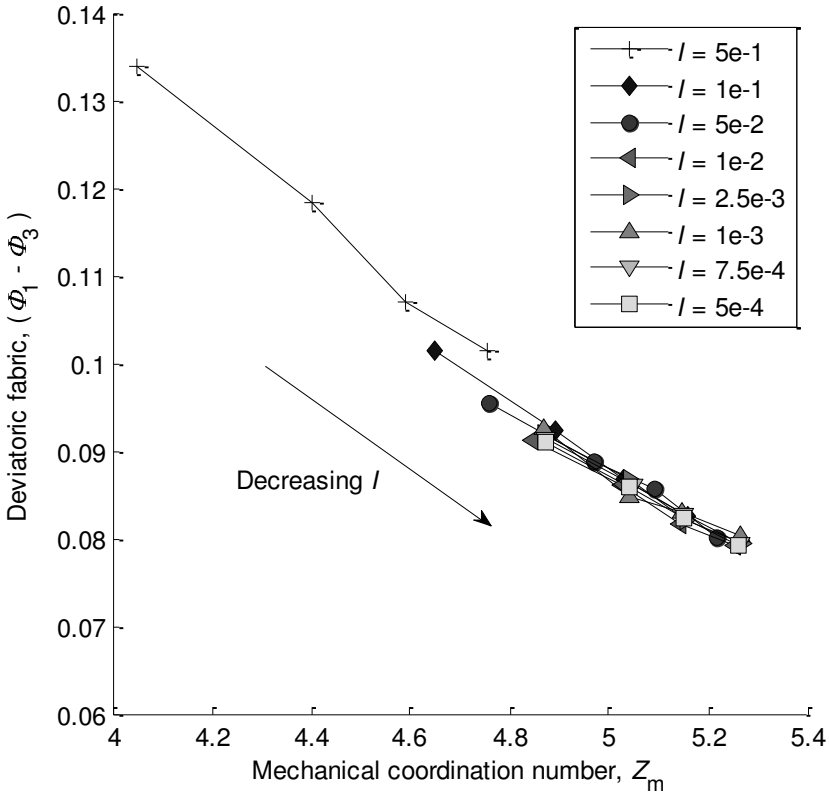

(a) Φ_1- Φ_3 against Z_m at critical state for different values of I

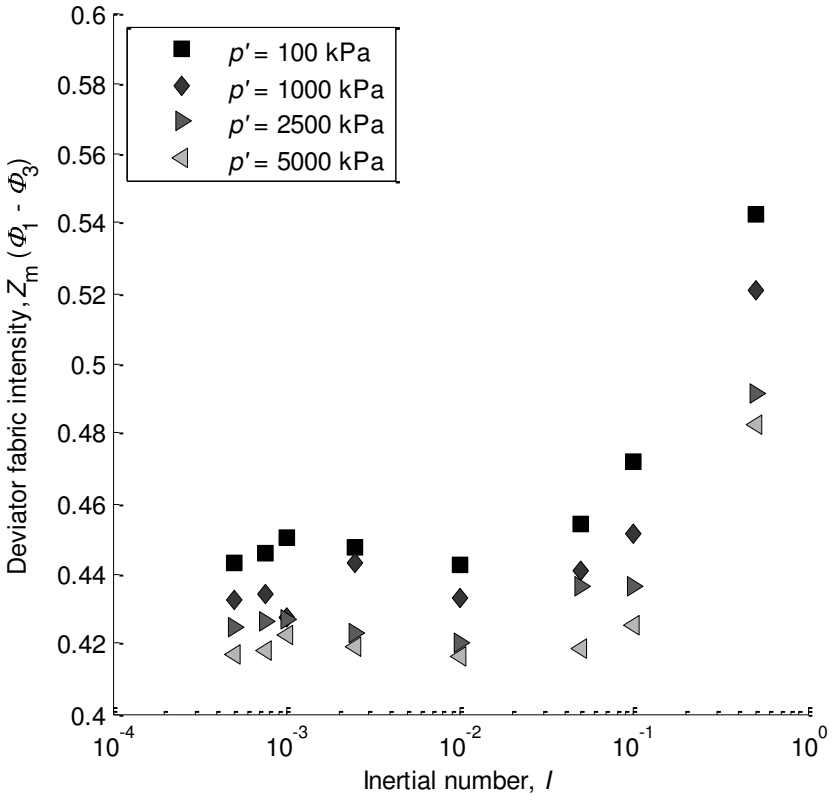

(b) Fabric intensity at critical state against I for different values of p'

Figure 6. (Φ_1- Φ_3)-Z_m relationships at the critical state

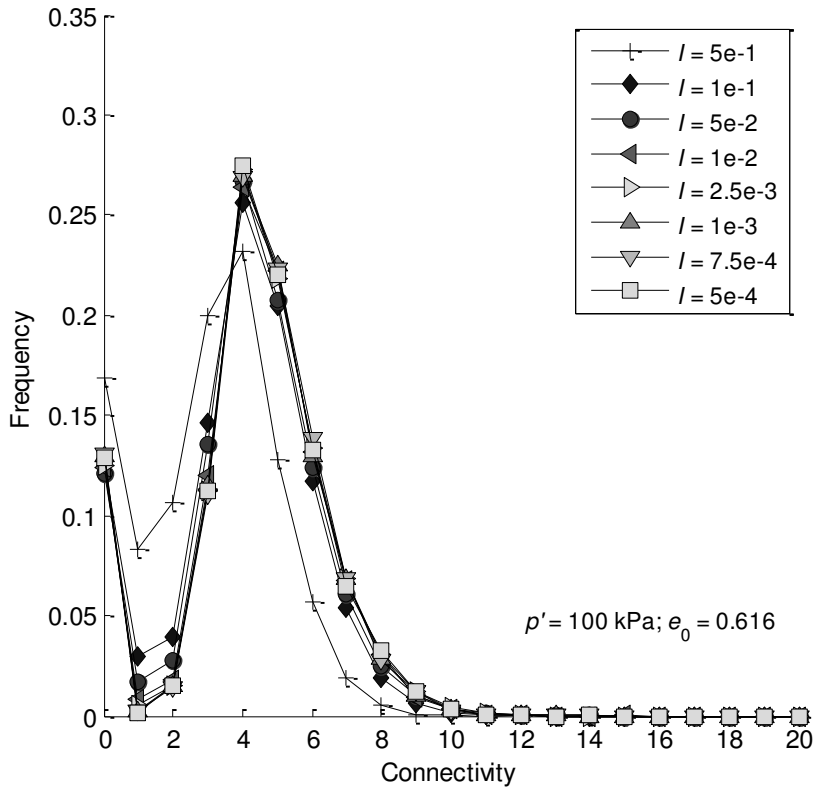

(a) Frequency plot of connectivity for p' = 100 kPa, e_0 = 0.616

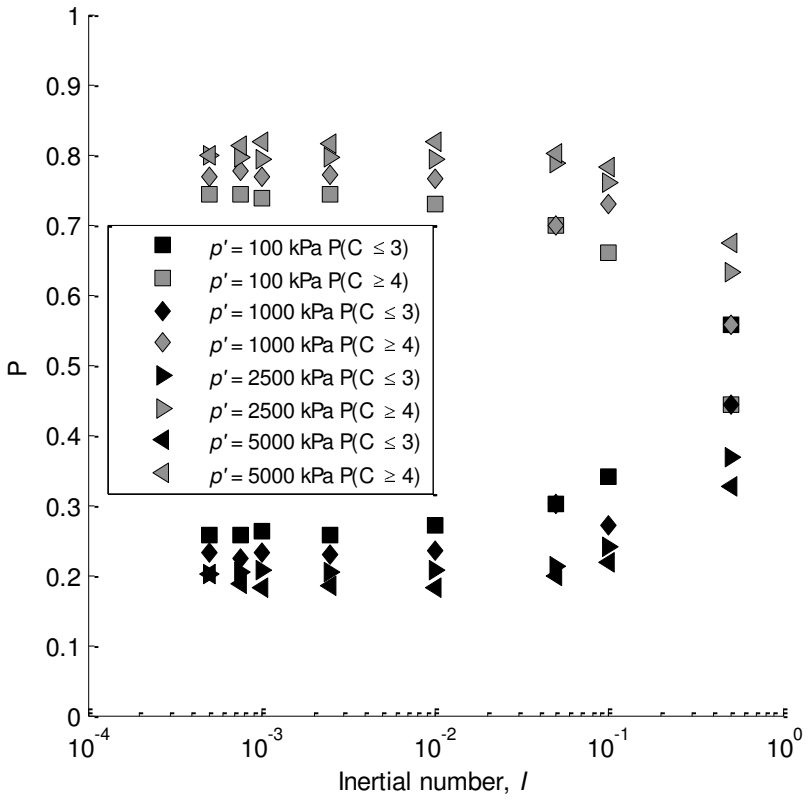

(b) Probability of connectivity P($C \leq 3$) and P($C \geq 4$) for various p'

Figure 7. Connectivity at the critical state.

Table 1. Summary of constant-p' triaxial simulations.

p'(kPa)	e_0	Strain rate (1/s) , $d\varepsilon_1/dt$ and $d\varepsilon_3/dt$ for different I and p'											
		I = 5e-1			I = 1e-1			I = 5e-2			I = 1e-2		
		$d\varepsilon_1/dt$	min $d\varepsilon_3/dt$	max $d\varepsilon_3/dt$	$d\varepsilon_1/dt$	min $d\varepsilon_3/dt$	max $d\varepsilon_3/dt$	$d\varepsilon_1/dt$	min $d\varepsilon_3/dt$	max $d\varepsilon_3/dt$	$d\varepsilon_1/dt$	min $d\varepsilon_3/dt$	max $d\varepsilon_3/dt$
100	0.616	500.7	-898.1	-264.2	100.1	-182.3	-50.4	50.1	-88.6	-24.6	10.0	-18.1	-4.9
1000	0.611	1583.2	-2938.8	-830.8	316.6	-572.2	-153.8	158.3	-289.5	-77.0	31.7	-55.4	-15.3
2500	0.649	2503.3	-4488.4	-596.6	500.7	-858.1	-140.9	2503.3	-430.7	-73.6	250.3	-89.2	-14.9
5000	0.596	3540.2	-6145.9	-1884.4	708.0	-1228.1	-358.2	354.0	-621.7	-178.6	70.8	-121.4	-35.9

		I = 2.5e-3			I = 1e-3			I = 7.5e-4			I = 5e-4		
		$d\varepsilon_1/dt$	min $d\varepsilon_3/dt$	max $d\varepsilon_3/dt$	$d\varepsilon_1/dt$	min $d\varepsilon_3/dt$	max $d\varepsilon_3/dt$	$d\varepsilon_1/dt$	min $d\varepsilon_3/dt$	max $d\varepsilon_3/dt$	$d\varepsilon_1/dt$	min $d\varepsilon_3/dt$	max $d\varepsilon_3/dt$
		2.5	-4.6	-1.2	1.0	-1.8	-0.5	0.8	-1.4	-0.4	0.5	-0.9	-0.2
		7.9	-13.4	-3.8	3.2	-5.8	-1.5	2.4	-4.1	-1.1	1.6	-2.9	-0.8
		12.5	-22.3	-3.8	5.0	-8.7	-1.5	3.8	-6.4	-1.1	2.5	-4.4	-0.8
		17.7	-30.1	-9.0	7.1	-12.4	-3.6	5.3	-9.1	-2.7	3.5	-6.1	-1.8

* $d\varepsilon_1/dt$ constant during shearing stage

** $d\varepsilon_3/dt$ variable during shearing stage